Predicting Human Tumor Drug Concentrations from a Preclinical Pharmacokinetic Model of Temozolomide Brain Disposition

Qingyu Zhou,[1] Ping Guo,[1] Gary D. Kruh,[2] Paolo Vicini,[3] Xiaomin Wang,[1] and James M. Gallo[1]

Abstract

Purpose: Knowledge of drug concentrations in tumors is critical for understanding the determinants of drug accumulation in tumors. Because significant obstacles prevent making these measurements in humans, development of a predictive pharmacokinetic model would be of great value to the translation of preclinical data to the clinic. Our goal was to show how the latter could be achieved for temozolomide, an agent used in the treatment of brain tumors, using an orthotopic brain tumor model in rats.

Experimental Design: Rats bearing i.c. tumors received 20 mg/kg i.v. of temozolomide followed by the subsequent measurement of serial plasma, cerebrospinal fluid (CSF), normal brain, and brain tumor temozolomide concentrations. The resultant data provided the framework to develop a hybrid physiologically based pharmacokinetic model for temozolomide in brain. The preclinical pharmacokinetic model was scaled to predict temozolomide concentrations in human CSF, normal brain, and brain tumor, and through a series of Monte Carlo simulations, the accumulation of temozolomide in brain tumors under conditions of altered blood-brain barrier permeability, fractional blood volume, and clinical dosing schedules was evaluated.

Results: The developed physiologically based pharmacokinetic model afforded a mechanistic and accurate prediction of temozolomide brain disposition in rats, which through model scale-up procedures accurately predicted the CSF/plasma area under the drug concentration-time curve ratios of 0.2 reported in patients. Through a series of model simulations, it was shown that the brain tumor accumulation of temozolomide varied substantially based on changes in blood-brain barrier permeability and fractional tumor blood volume but minimally based on clinical dosing regimens.

Conclusions: A physiologically based pharmacokinetic modeling approach offers a means to translate preclinical to clinical characteristics of drug disposition in target tissues and, thus, a means to select appropriate drug dosing regimens for achieving optimal target tissue drug concentrations.

Current drug development paradigms for moving anticancer agents into the clinic involve the identification of promising candidates based on measurements of their activities as assessed from measurements of tumor size in rodent xenograft models. The lack of detailed pharmacokinetic-pharmacodynamic studies that measure drug disposition and dynamics in tumors is a limitation in providing a quantitative framework to translate preclinical pharmacologic data to patients. This deficiency in part is attributed to the absence of a pharmacokinetic modeling strategy that links preclinical and clinical data. For example, such a model could predict drug concentrations in brain tumors, the latter of which are particularly difficult to assess in patients, and thereby provide a basis to adjust drug schedules. The problem of measuring drug concentrations in human brain tumors highlights a void in data on drug disposition in all human tumors (i.e., the target site). To address this issue, and cognizant that direct measurement of drug concentrations in human tumors will continue to be difficult to achieve, we sought to develop a predictive pharmacokinetic model. As a probe for these studies, we used temozolomide, an agent that is effective for treating gliomas (1, 2), and measured its concentration-time profiles in cerebrospinal fluid (CSF), normal brain, and brain tumor tissues in a rat orthotopic brain tumor model. Although the systemic pharmacokinetic properties of temozolomide are well characterized in patients (2, 3), and efficient central nervous system penetration is anticipated due to its relatively low plasma protein binding and high lipophilicity (4), the amount of drug reaching brain tumors in patients is unknown. This deficiency provided the impetus to develop a comprehensive preclinical pharmacokinetic model of temozolomide disposition in brain that subsequently could be scaled to predict human brain temozolomide concentrations. Such a pharmacokinetic model would not only offer insights on drug accumulation in target tissues

Authors' Affiliations: [1]Department of Pharmaceutical Sciences, School of Pharmacy, Temple University; [2]Medical Science Division, Fox Chase Cancer Center, Philadelphia, Pennsylvania; and [3]Department of Biomedical Engineering, University of Washington, Seattle, Washington

Received 3/20/07; revised 4/23/07; accepted 4/27/07.

Grant support: NIH grants CA72937 and CA85577 (J.M. Gallo).

The costs of publication of this article were defrayed in part by the payment of page charges. This article must therefore be hereby marked *advertisement* in accordance with 18 U.S.C. Section 1734 solely to indicate this fact.

Requests for reprints: James M. Gallo, Department of Pharmaceutical Sciences, School of Pharmacy, Temple University, 3307 North Broad Street, Philadelphia, PA 19140. Phone: 215-707-9699; Fax: 215-707-9409; E-mail: jmgallo@temple.edu.

doi:10.1158/1078-0432.CCR-07-0658

but also further offer a quantitative basis to design and adjust therapies. The potential of a preclinical mechanistic pharmacokinetic model to serve as a foundation to assess target organ drug distribution in patients represents a procedure that could be applied to other drugs and tumor types and could relieve a significant bottleneck in the drug development process.

Materials and Methods

Materials

Temozolomide was generously provided by Schering-Plough Research Institute (Kenilworth, NJ). All other chemicals, solvents, and materials were obtained from commercial sources.

Adult male athymic nude rats (*rnu/rnu*) were purchased from Taconic Farms. The care and use of animals was approved by the Institutional Animal Care and Use Committee in accordance with NIH guidelines.

Intracerebral glioma model

A previously described orthotopic rat model of human glioma was used throughout the investigations (5, 6). Male athymic rats (body weight, 190-240 g) were divided into two groups: group A, which had one guide cannula implanted in the left caudate putamen and the other in the right lateral ventricle in each animal, and group B, which had one guide cannula implanted in the left caudate putamen and the other one contralaterally in the right caudate putamen in each animal. The stereotaxic implantation of microdialysis guide cannulas was done according to our previously reported method with some modifications (5, 7). In brief, anesthetized animals were secured in a stereotaxic instrument, and a 1.5-cm longitudinal incision was made to expose the skull. Small holes were drilled into the skull for the placement of the guide cannula and two stainless steel anchor screws. The two guide cannulas, each fitted with a dummy probe, were then fixed to the skull using dental cement. The skin was sutured around the dental cement. Using a sterile 10-μL Hamilton syringe with a 26-gauge needle attached to the stereotaxic frame, SF188 vascular endothelial growth factor glioma cells (4×10^5) in 4 μL saline were injected 5.5 mm deep into the left caudate putamen over a 1-min period. After surgery, animals were returned to their cages and received a regular rat diet and water *ad libitum*. Animal body weight was measured once every 2 days throughout the study period. At the end of the pharmacokinetic experiment, the brains were taken out and sagittal brain sections were made to verify the placement of the probes in the desired locations (i.e., CSF, normal brain, and brain tumor).

Single-dose temozolomide administration and blood sampling

Because the size of the i.c. tumor could not be monitored, the pharmacokinetic experiment was conducted in tumor-bearing animals exhibiting a total weight loss of 10 gm over 2 consecutive days (5). One day before administration of temozolomide, the rats were cannulated under light anesthesia with isoflurane with polyethylene tubes in the right femoral vein and femoral artery for drug administration and blood sampling, respectively. Temozolomide (dissolved in 25% DMSO) at a dose of 20 mg/kg (equivalent to 222 mg/m^2; ref. 8) was given as a 10-min i.v. infusion to each animal. Blood samples of 100 μL were taken at predose, 5, 10, 20, and 40 min and 1, 1.5, 2, 3, 4, 5, 6, and 8 h after the start of infusion. Blood drawn was replaced with 50 μL of heparinized saline (10 units/mL) after each collection to avoid volume depletion. Plasma was separated by centrifugation and then stored at -80°C until analysis.

Tumor microdialysis

On the day of the experiment, the dummy cannulas located in the brain were replaced with CMA/12 dialysis probes with a membrane length of 2 mm. Before the administration of temozolomide, the probes were perfused at a rate of 2 μL/min with an artificial CSF [145 mmol/L NaCl, 1.2 mmol/L $CaCl_2$, 2.7 mmol/L KCl, 1.0 mmol/L $MgCl_2$ (pH 6.2)] containing 200 ng/mL temozolomide to determine the *in vivo* probe recovery for temozolomide using the retrodialysis method described elsewhere (9). Following the calibration of dialysis probes, a washout period of 40 min with blank artificial CSF before temozolomide administration was allowed to remove temozolomide from the system. Microdialysate samples were collected at 10-min intervals for 6 h after temozolomide administration and then stored at -80°C until analysis. The flow rate was maintained at 2 μL/min during the washout and sample collection periods. Unbound temozolomide concentrations in the extracellular fluid or CSF were calculated as the concentrations in the microdialysate from each brain region divided by the *in vivo* relative recovery of the microdialysis probe obtained from the same region during retrodialysis. The percentage relative recovery of temozolomide from the lateral ventricle, normal brain, and brain tumor regions were 17.2 ± 6.8, 15.8 ± 5.7, and 18.5 ± 8.8, respectively.

Quantitative analysis of temozolomide

Temozolomide concentrations in the plasma and tumor microdialysate were quantitated using an API 4000 electrospray ionization liquid chromatography tandem mass spectrometry (Applied Biosystems) as described previously (10). Briefly, temozolomide was extracted from plasma samples following the addition of internal standard dacarbazine and deproteinization with methanol. An aliquot of tumor microdialysate added to the internal standard was directly injected onto the liquid chromatography tandem mass spectrometry system. The liquid chromatography system consisted of a C18 guard cartridge (4.0 × 2.0 mm; Phenomenex) and a Luna C18 analytical column (50 × 2.0 mm, 3 μm particle size; Phenomenex). Elution was carried out with an isocratic mobile phase consisting of acetonitrile/0.5 mmol/L ammonium formate containing 0.1% formic acid (8:92 and 4:96 v/v, for plasma and microdialysate samples, respectively) at a flow rate of 0.2 mL/min. The instrument was operated in the positive ion scan mode, monitoring the ion transitions from m/z 195.1→137.9 for temozolomide and m/z 183.2→123.3 for dacarbazine with a dwell time of 800 ms for each ion transition. The low limit of quantification was 9 and 8 ng/mL for temozolomide in plasma and microdialysate, respectively. The intra-assay and interassay precisions were all <15%, and the accuracy expressed as the percentage error was within the range of ±15% and ±20% for plasma and tumor microdialysate, respectively.

Pharmacokinetic analysis

Preclinical physiologically based models of temozolomide brain disposition. A sequential approach was used to develop physiologically based pharmacokinetic models of temozolomide in individual animals in both groups A and B. In the first step, a compartmental model was fit to the observed plasma temozolomide concentration-time data in each animal using maximum likelihood optimization (11, 12). The resultant best-fit models were then cast as forcing functions that described the plasma temozolomide concentration input into brain tumor (groups A and B), CSF (group A), and normal brain (group B). Each brain region was defined by one or more compartments and fit to individual temozolomide concentration-time profiles in brain tumor and CSF (group A), and brain tumor and normal brain (group B). Once again, the maximum likelihood optimization procedure is used to select the best-fit compartmental model for each brain region. It was desired to combine the models for groups A and B so that a single comprehensive brain model of temozolomide could be obtained. To achieve this, a population approach was implemented, first to estimate population mean variables for groups A and B, and then as a combined population consisting of both groups A and B. The population mean variables for group A would provide Bayesian prior estimates for the CSF model, whereas group B would provide analogous prior estimates for the normal brain compartment. The model structures in CSF, normal brain, and brain tumor compartments were composed of mass balance equations for unbound temozolomide, the measured species by microdialysis.

Scale-up of the preclinical model to humans. Two approaches were used to scale-up the preclinical model of temozolomide to predict human CSF temozolomide concentrations. The first, referred to as the naive predictor, replaced the forcing function used in rats with one derived from available human plasma temozolomide data obtained following oral administration of temozolomide to patients, which is based on a simple one-compartment model with first-order absorption and elimination (13). The naive predictor coupled the human forcing function directly to the rat model for the CSF compartment only.

The second scale-up procedure linked the human forcing function, exactly the one used in the naive predictor, to a human model for temozolomide disposition in CSF, which used an equivalency between the ratio of the output/input variables (i.e., K_{out}/K_{in}) determined by Ostermann et al. (13) and the ratio of the physiologically equivalent output/input variables determined in our rat model. By setting the ratio of the input-output variables (i.e., K_{out}/K_{in}) determined by Ostermann et al. (13) to the ratio of the physiologically equivalent input-output variables determined in our rat model, the following equation is obtained:

$$\frac{K_{out}}{K_{in}} = \frac{\left[PA^{r}\frac{SA^{h}}{SA^{r}} + Q^{h}_{csf} + CL^{r}_{csf}\frac{V^{h}_{csf}}{V^{r}_{csf}}\right]/V^{h}_{csf}}{f^{h}_{u}\left(\frac{PA^{r}}{V^{h}_{p}}\right)\frac{SA^{h}}{SA^{r}}}$$

where K_{out} is CSF to plasma efflux rate constant (h^{-1}); K_{in} is the plasma to CSF influx rate constant (h^{-1}); PA^{r} is the permeability-area product in rats (mL/h); Q^{h}_{csf} is the CSF bulk flow rate in humans (mL/h); CL^{r}_{csf} is the temozolomide clearance from CSF in rats (mL/h); V^{h}_{csf} is the volume of CSF in humans (mL); V^{r}_{csf} is the volume of CSF in rats (mL); f^{h}_{u} is the fraction of unbound temozolomide in human plasma; and $\frac{SA^{h}}{SA^{r}}$ is the ratio of human to rat choroid plexus surface area.

From the above equation, one can solve for the ratio of the surface area of the choroid plexus in humans to rats, $\frac{SA^{h}}{SA^{r}}$, because all other values in the above equation are known and, subsequently, use this value to calculate the permeability-area product in humans, PA^{h}, as follows:

$$PA^{h} = PA^{r}\frac{SA^{h}}{SA^{r}}$$

Other than the permeability-area product, the human scaled CSF model required estimates for the CSF bulk flow rate, which is readily available from the literature (14), and CL^{h}_{csf} When it is assumed that drug clearance is first order or dose independent, it is equal to the product of a first-order rate constant for elimination and the volume of distribution. Specifically, $CL^{r}_{csf} = k^{r}_{csf}V^{r}_{csf}$ and $CL^{h}_{csf} = k^{h}_{csf}V^{h}_{csf}$ where CL^{h}_{csf} is the temozolomide clearance from the CSF in humans (h) and k^{r}_{csf} and k^{h}_{csf} are the first-order rate constants for temozolomide elimination from the CSF in rats (r) and humans (h), respectively.

Given that the clearance of temozolomide from CSF (CL^{r}_{csf} and CL^{h}_{csf}) is primarily associated with the pH-dependent conversion of temozolomide to metabolite 3-methyl-(triazen-1-yl)imidazole-4-carboximide, it was assumed that $k^{r}_{csf} = k^{h}_{csf}$; therefore, following substitution, CL^{h}_{csf} can readily be calculated as follows:

$$CL^{h}_{csf} = CL^{r}_{csf}\frac{V^{h}_{csf}}{V^{r}_{csf}}.$$

Both the naive and scaled predictor models can simulate temozolomide plasma and CSF concentrations given any dosing schedule; however, for comparative purposes, we chose an oral temozolomide dose of 200 mg/m^2 (mean bovine serum albumin, 1.8 m^2) and subsequently calculated the area under the drug concentration-time curve (AUC) from time 0 to 24 h in plasma (AUC_p) and CSF (AUC_{csf}) and the ratio AUC_{csf}/AUC_p.

Based on the successful scale-up of the CSF model, the scaled model for human CSF temozolomide disposition was expanded to include the normal brain and brain tumor. The model structures for the normal brain and brain tumor compartments were set equivalent to those used in the preclinical models derived from groups A and B. The variables characterizing the influx and efflux of temozolomide across the blood-brain barrier (BBB) were set equal to those in the preclinical model and represented membrane permeability and temozolomide degradation in the extravascular compartment as the net efflux of intact temozolomide is appreciably less than the influx. The physiologic variables of blood flow in normal brain (15) and brain tumor (16), and fractional vascular volumes (17) were obtained from the literature. The human model for temozolomide disposition in brain, consisting of CSF, normal brain, and brain tumor compartments, was used to simulate or predict temozolomide concentration-time profiles in each compartment under three clinically used dosing schedule: standard (200 mg/m^2 daily × 5 days), compressed (200 mg/m^2 every 8 h for 5 doses), and extended (75 mg/m^2 daily × 21 days). Unlike CSF, normal brain and brain tumor temozolomide measurements in patients are unavailable; thus, there is no direct means to validate model predictions in these tissues; however, assessments were made on how changes in the model variables affected the predicted temozolomide concentrations and associated AUC values. To accomplish this, Monte Carlo simulations were conducted by varying either the brain tumor BBB influx variable or the fractional volume of the vascular compartment based on dynamic contrast-enhanced magnetic resonance imaging (MRI) data in brain tumor patients (17), which showed that BBB permeability (often referred to as K_{trans}) varied ~4-fold depending on the tumor grade, and the regional brain tumor volume varied ~6-fold relative to normal brain. These degrees of variability were incorporated into the human model for temozolomide in brain by allowing the brain tumor fractional vascular volume to vary from 0.02 to 0.12 and by adjusting the brain tumor BBB permeability by a factor from 0.6 to 2.4, using the Monte Carlo simulator feature of PopKinetics (12). The number of simulations was set at 200 for both conditions, which yielded for each unique value of BBB permeability and fractional vascular volume a predicted temozolomide concentration-time profile in each compartment. The AUC values in brain tumor (AUC_{bt}) were tabulated and expressed as the ratio to the AUC_p.

Statistical analysis

Statistical analyses were done using NCSS 2004 program (Number Cruncher Statistical Systems). Paired t tests were used to compare AUC_{csf} versus AUC_{bt}, and AUC_{nb} versus AUC_{bt} in groups A and B, respectively. In addition, t tests were used to compare systemic pharmacokinetic variables (i.e., CL and V) based on the mean values from two independent groups. A two-sided P value of <0.05 was considered statistically significant.

Results

Development of the preclinical pharmacokinetic model of temozolomide. A compartmental modeling analysis applied to individual rats in groups A and B revealed a one-compartment model best-fit the observed plasma temozolomide concentrations. There were no statistically significant differences found in C_{max}, AUC_p, $t_{1/2}$, CL, and V for temozolomide between these two groups (Table 1), which was expected because only the location of the microdialysis probes differed between groups A and B. Thus, the systemic exposure (i.e., AUC_p), elimination rate (CL), and volume of distribution (V) were equivalent in the two groups.

Once the one-compartment model was defined for each animal from the plasma concentration-time profiles of temozolomide, it was set as a forcing function in compartmental models that were fit to individual rat temozolomide brain concentrations. Definition of a constant forcing function in the

Table 1. Pharmacokinetic variables of temozolomide based on plasma concentrations in athymic rats bearing i.c. SF188 V+ human glioma xenografts after i.v. administration of 20 mg/kg temozolomide

Variables	Group A (n = 10)*			Group B (n = 9) †		
	Plasma ‡	CSF§	Tumor§	Plasma ‡	Normal brain§	Tumor§
T_{max} (h)	0.16 ± 0.07	0.667 ± 0.161	0.634 ± 0.208	0.14 ± 0.04	0.491 ± 0.145	0.363 ± 0.085
C_{max} (μg/mL)	20.2 ± 3.72	3.38 ± 2.19	2.80 ± 1.14	21.9 ± 6.14	2.66 ± 1.31	4.01 ± 2.59
AUC (μg·h/mL)	24.4 ± 5.63	4.51 ± 2.65	4.62 ± 2.59	25.6 ± 5.74	5.36 ± 1.93	5.14 ± 4.26
$t_{1/2}$ (h)	0.89 ± 0.07	0.860 ± 0.206	0.770 ± 0.246	0.90 ± 0.05	0.974 ± 0.219	0.975 ± 0.244
CL (L/h/kg)	0.86 ± 0.18			0.83 ± 0.24		
V (L/kg)	1.10 ± 0.26			1.07 ± 0.29		
AUC ratios‖						
AUC_{bt}/AUC_p			0.193 ± 0.096			0.193 ± 0.135
AUC_{csf}/AUC_p		0.202 ± 0.150				
AUC_{nb}/AUC_p					0.223 ± 0.129	

NOTE: Data are represented as the mean ± SD.
*Each animal had a microdialysis probe inserted in the lateral ventricle and i.c. tumor.
† Each animal had a microdialysis probe inserted in the normal cerebrum and i.c. tumor.
‡ Pharmacokinetic variables were estimated using a one-compartmental model.
§Pharmacokinetic variables were estimated using noncompartmental methods except for the AUC, which was estimated using the hybrid model.
‖AUC ratios were calculated from the model-estimated unbound temozolomide brain concentrations and the total temozolomide concentrations in plasma.

development of the brain models minimized the number of variables that had to be estimated and facilitated attainment of a robust variable set. In addition to the forcing function, several other variables were fixed (Table 2) to previously reported values (blood flows, CSF bulk flow rate, tissue volumes, and plasma protein binding), which left PA_{csf}, CL_{csf}, K_{btvev}, and K_{btevv} to be estimated in group A, whereas for group B, the estimated variables were K_{nbvev}, K_{nbevv}, K_{btvev}, and K_{btevv}. Once the models for A and B were successfully defined, they were combined into a single brain model, in which Bayesian variable estimation was used to provide final estimates for PA_{csf}, CL_{csf}, K_{nbvev}, and K_{nbevv}. In the combined brain model, K_{btvev}, and K_{btevv} could be estimated for each animal because they all had observed temozolomide measurements in brain tumor. The final preclinical model and model variables of temozolomide brain disposition is provided in Fig. 1A and Table 2, respectively. An indication of the quality of the model fit is provided in Fig. 1B to D that shows the mean predicted

Table 2. Pharmacokinetic model variables for the rat and human temozolomide brain disposition models

Variable symbol (units)	Definition	Value*	
		Rat model	Human model
Species-dependent pharmacokinetic variables			
K_{01} (h^{-1})	Elimination rate constant from central compartment	0.776 ± 0.051	0.333
V (mL)	Volume of distribution	233 ± 68.3	30,300
PA_{csf} (mL/h)	Permeability-area product in CSF	0.283 ± 0.173	175
CL_{csf} (mL/h)	Clearance from CSF	0.756 ± 0.313	529
Species-independent pharmacokinetic variables			
K_{nbvev} (h^{-1})	Vascular to extravascular influx rate constant in normal brain	106 ± 76.9	106
K_{nbevv} (h^{-1})	Extravascular to vascular efflux rate constant in normal brain	7.56 ± 5.48	7.56
K_{btvev} (h^{-1})	Vascular to extravascular influx rate constant in brain tumor	81.3 ± 125	81.3
K_{btevv} (h^{-1})	Extravascular to vascular efflux rate constant in brain tumor	14.9 ± 13.2	14.9
Physiologic and anatomic variables from the literature			
f_u	Unbound fraction in plasma	0.80	0.86
Q_{csf} (mL/h)	Bulk flow rate from CSF	0.132	30
V_{csf} (mL)	Volume of the CSF compartment	0.2	140
Q_{nb} (mL/h)	Normal brain blood flow	99.7	42,000
f_{Bvnb}	Normal brain fractional blood volume	0.02	0.02
V_{nb} (mL)	Normal brain total volume	1.146	1,450
Q_{bt} (mL/h)	Brain tumor blood flow	3.86	2,400
f_{Bvbt}	Brain tumor fractional blood volume	0.05	0.05
V_{bt} (mL)	Brain tumor total volume	0.119	50

*Values estimated by maximum likelihood optimization were reported as mean ± SD; all other variables were fixed.

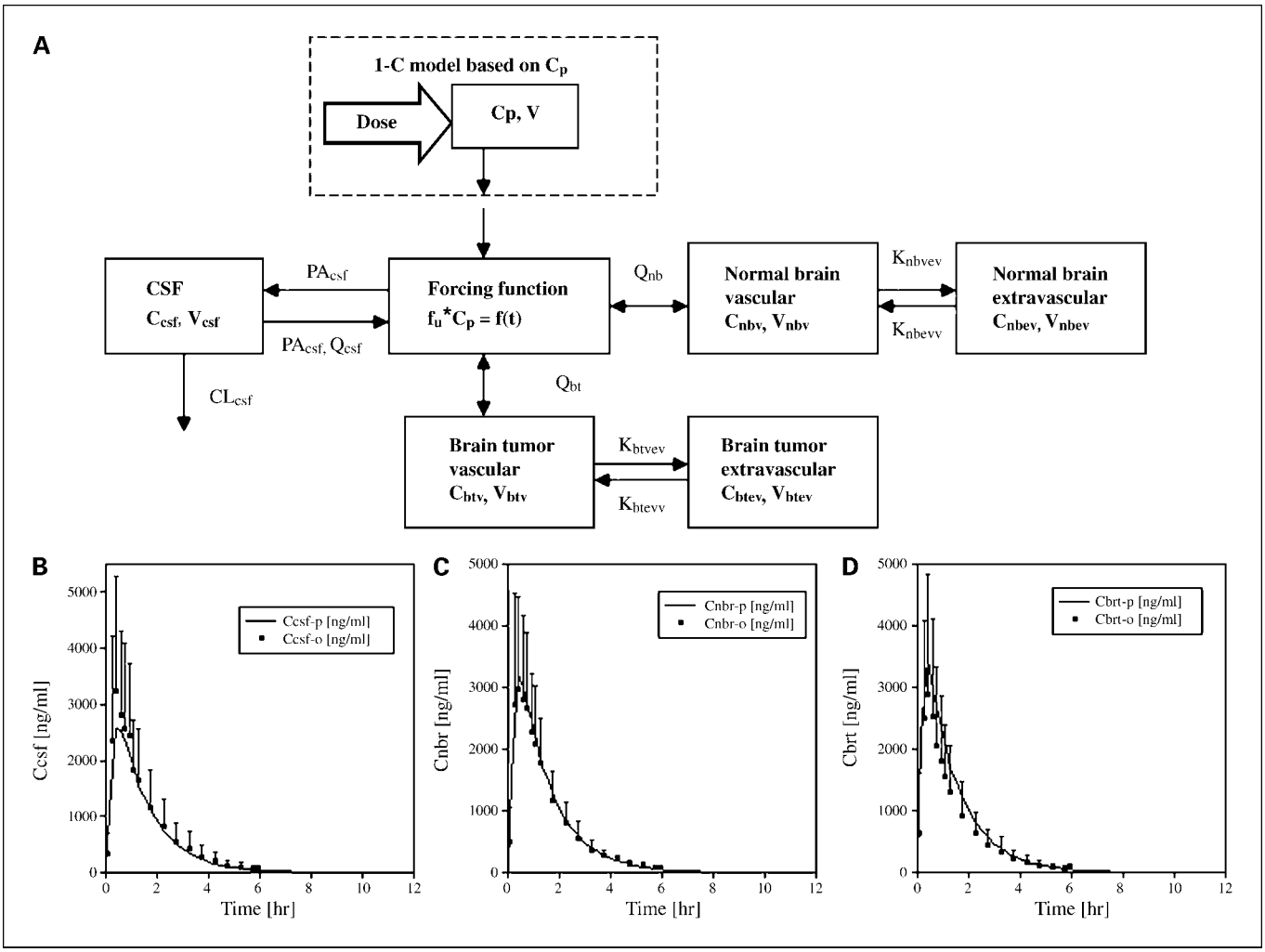

Fig. 1. *A,* schematic presentation of the hybrid physiologically based pharmacokinetic model of temozolomide in brain. The dose input for rats was i.v., whereas for humans, it was oral. The structure of the brain model is the same in rats and human, and the associated definition of the model symbols and variable values are provided in Table 2. Points, mean observed (■) and model-predicted (—) temozolomide concentration-time profiles in CSF (*B*), normal brain (*C*), and brain tumor (*D*) after i.v. administration of temozolomide at a dose of 20 mg/kg to athymic rats bearing i.c. SF188 vascular endothelial growth factor gliomas; bars, SD.

temozolomide concentrations in CSF, normal brain, and brain tumor compared with the mean (SD) of the observed values.

Nature of the preclinical pharmacokinetic model of temozolomide. The three brain regions represented in the model are the CSF, normal brain, and brain tumor. The CSF compartment is a single compartment that is most typical to describe drug distribution into CSF (14, 18) and was based on the measurements from group A. The CSF compartment is separated from the systemic central compartment by the blood-CSF barrier, which is formed by the tight junctions of adjacent epithelial cells known in the choroid plexus. Blood flow to the CSF is not a rate-limiting step for drug penetration because the vascular capillaries are fenestrated permitting drugs to have rapid access to the blood-CSF barrier. The influx into the CSF is controlled by the permeability-area product (PA_{csf}) that is associated with drug diffusion. The efflux of temozolomide from the CSF consists of three distinct processes: the equivalent PA_{csf} as used for influx, the bulk flow or convective transport of temozolomide (Q_{csf}), and a CSF clearance (CL_{csf}). The bulk flow elimination was set equal to its physiologic value reported previously in rats (14), whereas the two drug-dependent variables (PA_{csf} and CL_{csf}) were estimated from the observed temozolomide concentrations. The CSF clearance for temozolomide accounts for the pH-dependent conversion of temozolomide to metabolite 3-methyl-(triazen-1-yl)imidazole-4-carboximide, the penultimate DNA-alkylating species (19), which would be prevalent at the CSF pH of ~7.4. Based on the relative values of the three CSF processes (Table 2), it can be seen that $CL_{csf} > PA_{csf} > Q_{csf}$, which attests to the significance of temozolomide degradation in CSF. Interestingly, the permeability-area product was ~2-fold greater than bulk flow, which is attributed to the high lipophilicity of temozolomide.

The best-fit models for both normal brain and brain tumor temozolomide measurements consisted of two-compartment structures, which corresponded to a vascular compartment and an extravascular compartment that lumps the interstitial fluid and intracellular spaces (Fig. 1A). These models use either normal brain or brain tumor blood flow to deliver temozolomide to the vascular compartment that is separated from the extravascular compartment by the BBB, an important barrier to drug distribution and most likely to be altered by the presence of a brain tumor. By comparison of the normal brain (K_{nbvev})

and brain tumor (K_{btvev}) influx variable values (Table 2), it can be seen that transport of temozolomide was slightly accelerated (106 h^{-1} versus 81.3 h^{-1}) into normal brain relative to brain tumor, which may not have been anticipated based on the finding that the brain tumor BBB may be compromised and more permeable (20). However, at the same time, brain tumors are heterogeneous and depending on the location of sampling and degree of angiogenesis, BBB permeability can vary widely as seems to be the case given the large SD of K_{btvev} relative to K_{nbvev}. The two-compartment brain structures depicting a separate vascular and extravascular space facilitated scale-up of the model to humans as MRI analyses often characterize BBB permeability and the fractional vascular blood volume in brain tumors (17, 21). By experimental measurement of the total brain and brain tumor weights, and assuming a density of 1 gm/mL, the respective vascular and extravascular volumes were determined by assignment of literature values (22) to the fractional vascular volumes in normal brain and brain tumor, which were set equal to 0.02 and 0.05, respectively (Table 2).

The pharmacokinetic variables of temozolomide in brain are summarized in Table 1. The mean maximum concentrations of temozolomide in CSF, normal brain, and brain tumor occurred from ~0.4 to 0.7 h after the start of the infusion and were 12% to 18% of the peak plasma concentrations. The mean ratios of the brain (CSF, normal brain, and brain tumor) AUC values to the plasma AUC were ~0.20 as calculated from the model-estimated unbound temozolomide brain concentrations and the total temozolomide concentrations in plasma. Expressing the AUC ratios as such corresponds to the actual measured unbound temozolomide concentrations in CSF and brain interstitial fluid (i.e., normal brain and brain tumor) and total plasma temozolomide measurements. Even when one accounts for the low plasma protein binding of temozolomide in rats (20% bound; ref. 23), the brain AUC ratios (i.e., AUC_{csf}/AUC_p, AUC_{nb}/AUC_p, and AUC_{bt}/AUC_p) increase by 25% but are appreciably less than unity as one might expect for a drug that equilibrates by diffusion between plasma and a noneliminating tissue. For drugs that are substrates for membrane transporters that influence drug influx and efflux from a tissue, nonunity values for free drug distribution are likely (24); however, for temozolomide that is not known to undergo active transport, the lower brain/plasma AUC ratios most likely represent metabolism to metabolite 3-methyl-(triazen-1-yl)imidazole-4-carboximide. No statistically significant differences in the T_{max}, C_{max}, $t_{1/2}$, and AUC_{bt}/AUC_p values of temozolomide were found between groups A and B, and supports combining these groups for the final pharmacokinetic model of temozolomide.

Clinical pharmacokinetic model of temozolomide in CSF. The first step in constructing a human model for temozolomide disposition in brain concerned the development of a model for temozolomide in CSF. In this regard, both naive and scaled predictors revealed a model that agreed with the available human CSF temozolomide measurements of Ostermann et al. (13). For both the naive and scaled predictors, the forcing function that described temozolomide plasma concentration was set equal to the variables obtained by Ostermann et al. (Table 2; ref. 13). These variables agreed with those reported by others for temozolomide systemic pharmacokinetic properties following oral administration to patients (3). The naive and scaled CSF model predictions were quite similar (Fig. 2A) and were in agreement with temozolomide CSF concentrations obtained by Ostermann et al. (13), which ranged from 0.16 to 1.93 μg/mL. Moreover, both the naive and scaled predictors yielded values of the AUC_{csf}/AUC_p ratio to be 0.207 and 0.205, respectively, which was in close agreement with the ratio of 0.203 obtained by Ostermann et al. (13) at a dose of 200 mg/m^2. It was not specified by Ostermann et al. (13)

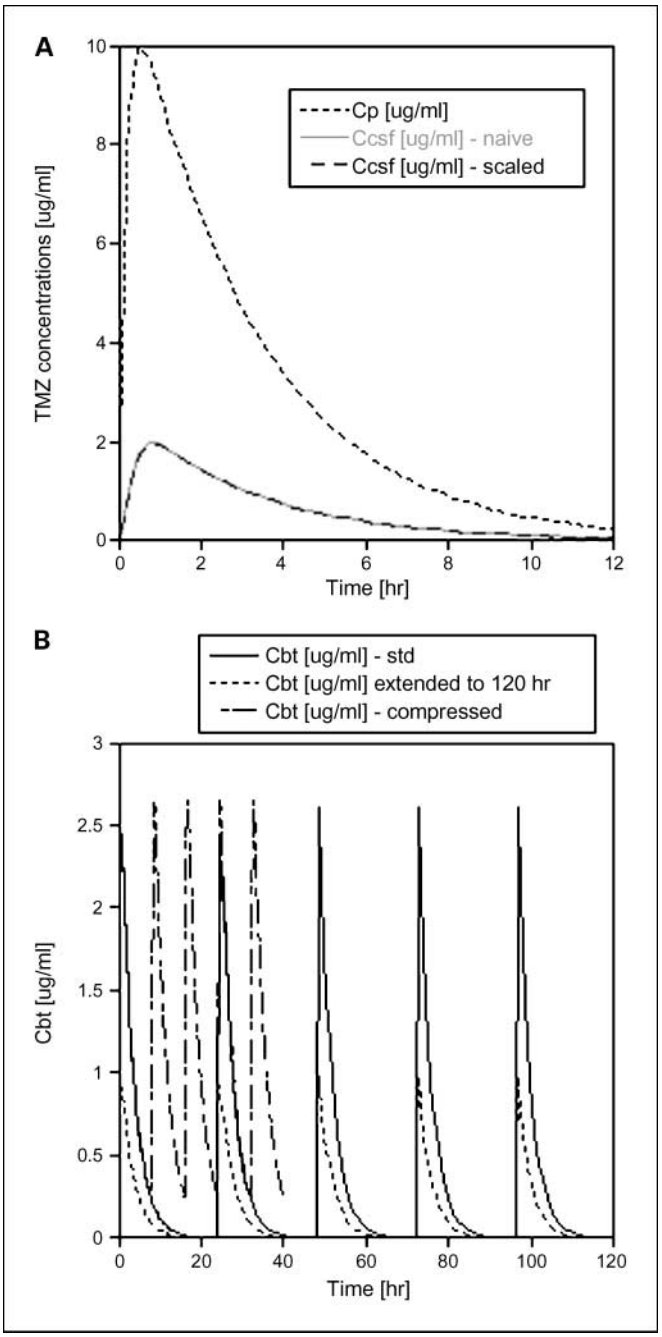

Fig. 2. *A,* human model-predicted plasma (·····) and CSF temozolomide concentrations using naive (—) and scaled (- -) model predictors. The CSF temozolomide concentrations for these two predictors closely overlap. *B,* human model-predicted temozolomide brain tumor concentrations comparing three different dosing regimens: standard (*std*; 200 mg/m^2 daily × 5 d every 28 d), compressed (200 mg/m^2 every 8 h for 5 doses every 28 d), and extended (75 mg/m^2 daily × 21 d every 28 d). The simulations are shown to 120 h, the end of the standard dosing cycle, for clarity. The model variables were those provided in Table 2.

whether temozolomide CSF concentrations represented total or unbound concentrations; however, because protein concentrations in CSF are exceedingly low (25), it is reasonable to assume that they are most indicative of unbound temozolomide concentrations as we measured in rats, and facilitates the comparison of the AUC_{csf}/AUC_p ratios. Although it was unexpected that the naive predictor did well, it can be attributed to the appropriateness of the rat as a model for the CSF disposition of temozolomide and its underlying mechanistic structure that accounts for drug diffusion, bulk flow transport, and degradation to metabolite 3-methyl-(triazen-1-yl)-imidazole-4-carboximide. The scaled CSF model also did well and was physiologically based. The crux of the scale-up technique was to determine the ratio of the human to rat surface area of the choroid plexus, which was subsequently used to scale the permeability-area product. Unlike data available on the surface area of the BBB that were fairly consistent (26), estimates of the surface area of the choroid plexus varied widely (27, 28) and can most likely be attributed to whether and how the microvilli on the apical border are measured. Our analysis estimated the ratio of the human to rat choroid plexus surface area to be ~600, which is of the same order as the ratio of the BBB in these same species (26). The complete procedure to scale the rat to the human CSF model also required values for the human clearance of temozolomide from the CSF and the bulk flow rate of CSF, which was estimated from the literature (14).

Clinical pharmacokinetic model of temozolomide in brain. Based on the validated CSF models, the next step to develop a complete brain model extended the physiologic approach to the normal brain and brain tumor compartments. To accomplish the latter, the structure of the preclinical model (Fig. 1A) was assumed to be equivalent in patients, with human physiologic variables being assigned values from the literature and the influx and efflux of temozolomide across the BBBs of normal brain and brain tumor being set equal to those determined in rats (see Materials and Methods; Table 2).

Using the base model variables (Table 2), a comparison of predicted human brain tumor temozolomide concentrations was made (Fig. 2B) following administration of three clinical treatment regimens: standard, compressed, and extended temozolomide dosing protocols. The total dose of temozolomide administered in the standard and compressed regimens was equal as were the total AUC_{bt} values, being ~44 μg h/mL. The compression of the five doses to 8-h intervals had a negligible effect on the accumulation of temozolomide in the tumor as essentially all the drugs are eliminated before the subsequent dose. Whether this more intense dosing schedule has a beneficial influence on the formation of DNA adducts cannot be predicted by the model at this time. The extended, 21 daily doses, temozolomide dosing schedule achieved the highest total AUC, being 70 μg h/mL, yet at the same time reached maximum brain tumor concentrations of >2-fold less than with the compressed and standard dosing schedules. One of the more important phenomenon shown by the simulations is that none of the dosing schedules produced drug accumulation in the tumor, and selection of one regimen over the others would have to be based on the formation and repair of lethal DNA adducts, drug toxicity, and convenience to patients.

Among the set of model variables, those associated with the brain tumor compartments were probed to see how changes in their values influenced predicted temozolomide brain tumor concentrations as these would most likely vary from patient to patient. Specifically, changes in the BBB influx (K_{btvev}) and the fractional vascular volume (f_{Bvbt}) were independently assessed using a Monte Carlo approach. These variables were of particular interest as it has been shown using dynamic contrast-enhanced MRI that the grading of a patient's brain tumor can be related to BBB permeability and the fractional blood volume in the tumor (17, 21, 29), both increasing in going from a tumor grade of I to III. From the Monte Carlo simulations that generate unique temozolomide brain concentration-time profiles for each value of K_{btvev} and f_{Bvbt}, the ratio of the AUC_{bt}/AUC_p was calculated and found to range several fold with peak values of ~0.6 (Fig. 3). The AUC_{bt} is based on extravascular brain tumor temozolomide concentrations; thus, the increase in AUC_{bt}/AUC_p with an increase in BBB influx is readily understandable; however, the increases in AUC_{bt}/AUC_p with increases in the fractional brain tumor volume require further scrutiny. As f_{Bvbt} increases, the volume of the extravascular space decreases, causing temozolomide concentrations, and accordingly AUC_{bt}, to increase because the amount of temozolomide in the extravascular space is confined to a smaller volume given a constant total volume of the brain tumor. These analyses indicate that temozolomide brain tumor concentrations and exposures can vary substantially based on the anatomic and physiologic state of the tumor. Based on the relationships between tumor grade and BBB permeability and fractional blood volume found by MRI, greater temozolomide exposures are expected as the severity of the brain tumor increases.

Discussion

Elucidating the pharmacokinetic profiles of chemotherapeutic agents in human tumors is not done. The numerous impediments to such practice include the limited availability of tumor samples after drug treatment and the likelihood that single drug concentration measurements may reveal little about the true extent of drug accumulation in the tumor. Another hurdle to the assessment of drug disposition in human tumors is that the current drug development strategy relies on semiempirical selection of drug dosing regimens that are predicated on preclinical efficacy studies, which are later supplemented with measurements of plasma drug concentrations and toxicity in patients. Reliance on these attributes as benchmarks for drug development could be altered if robust preclinical pharmacokinetic models predictive of drug disposition in target tissues in patients were available. Therefore, the goal of this investigation was to develop a comprehensive preclinical pharmacokinetic model of an anticancer drug in a target tissue and subsequently assess its ability to predict human brain temozolomide concentrations. To the best of our knowledge, this is the first study to successfully translate a preclinical pharmacokinetic model of drug disposition in an orthotopic tumor model to humans. The physiologically based pharmacokinetic approach was instrumental to the process and preserved the mechanistic aspects of drug transport in brain.

The pharmacokinetic modeling approach we used to characterize temozolomide brain disposition has been referred to as a hybrid technique (23), in that it combines a classic compartment model to describe plasma drug concentrations

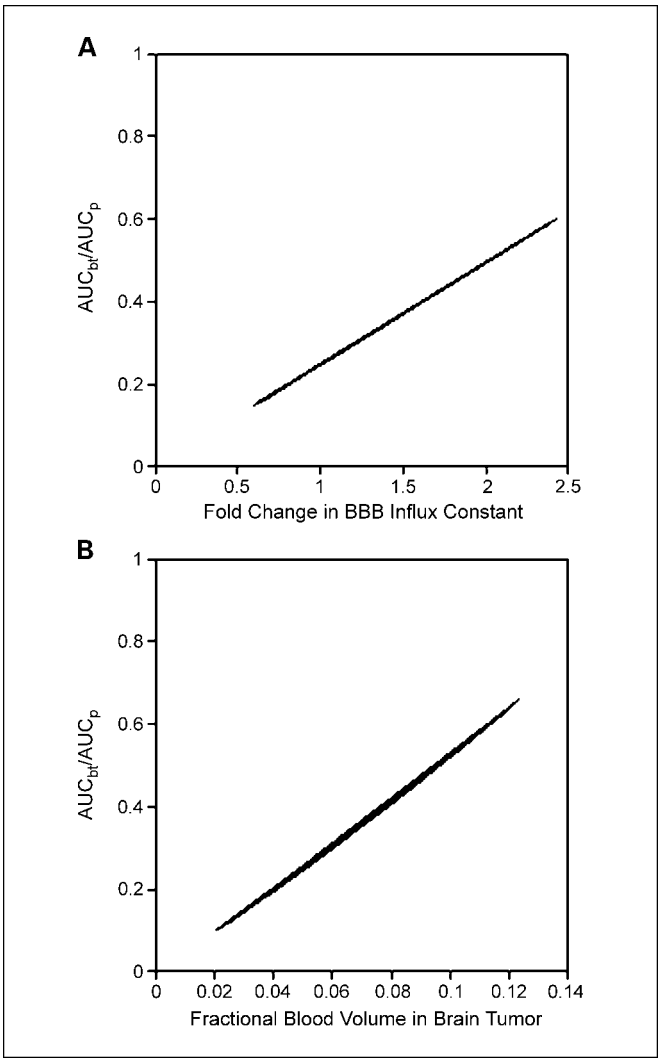

Fig. 3. Human predicted temozolomide AUC_{bt}/AUC_p due to changes in the brain tumor BBB influx rate constant (*A*) and changes in the fractional blood volume of the brain tumor (f_{Bvbt}; *B*). Changes in BBB influx were expressed as the fold change from 0.6 to 2.4 (*A*). f_{Bvbt} was varied from 0.02 to 0.12 (*B*). Using these ranges that were consistent with dynamic contrast-enhanced MRI data obtained in brain tumor patients (17), the Monte Carlo simulator of PopKinetics randomly generated 200 values of the BBB influx rate constant and f_{Bvbt} that were used to generate temozolomide concentration-time profiles and the associated AUC values.

with a physiologic mass balance approach to describe drug disposition in tissues. The hybrid technique eliminates the burdensome task of determining whole-body drug distribution by focusing on selected tissues of particular interest, yet at the same time retains the physiologic features of the organ. By retaining the physiologic characteristics of the brain in our model for temozolomide, we were afforded a means to scale the animal model to man and facilitate a mechanistic description of drug distribution. This mechanistic description of drug transport is highlighted in the CSF model for temozolomide that accounts for drug diffusion across the blood-CSF barrier, convective removal of the drug from the CSF via bulk flow, and clearance by pH-mediated conversion of temozolomide to metabolite 3-methyl-(triazen-1-yl)imidazole-4-carboximide. The two-compartment structures used for both normal brain and brain tumor permitted the vascular and extravascular compartments to be separated by the BBB, an important component of drug distribution and whose permeability is assessed in brain tumor patients by MRI as a means to classify the tumor grade (17, 21) and ultimately guide treatment. Overall, the preclinical hybrid physiologically based pharmacokinetic model for temozolomide in brain agreed with the observed temozolomide concentrations and formed the basis to scale to humans.

Animal-to-man scale-up of pharmacokinetic data have been conducted in two formats; one, as a drug development tool to predict human systemic pharmacokinetic characteristics, such as drug clearance and oral bioavailability (30, 31), and secondarily, as a means to predict tissue drug concentrations. In the former case, allometric equations based on animal body weight are the tools to estimate the human systemic pharmacokinetic variable. The scale-up of physiologically based pharmacokinetic models from animals to man is sparse (32), due to the inability to validate the predictions with human data and the lack of a standard methodology as seen with the allometric relationship. The lack of a standard methodology for scale-up of physiologically based pharmacokinetic models can be in part attributed to the unique organ structures and associated variables. For our temozolomide brain model, we concentrated on how to scale the rat model for CSF to man given the availability of human temozolomide CSF measurements (13). Both the naive and scaled predictors were in agreement with actual patient data (13), all yielding values of the AUC_{csf}/AUC_p to be ~ 0.2. An interesting and potentially significant implication of the human models for CSF is that "one-step" scaling (i.e., rat to human) was achieved without the often held premise that multiple animal species are needed to define animal-to-man extrapolations (33, 34). One-step scaling could expedite the development of other predictive pharmacokinetic models of drug disposition in target tissues. Based on the suitability of the CSF model predictions for temozolomide, the complete brain model was scaled to humans.

An attractive feature of our complete brain model for temozolomide is that it can be used to probe how various variables and dosing schedules affected temozolomide brain concentrations. Comparisons of the three clinically relevant temozolomide dosing protocols indicated that brain tumor temozolomide concentrations and exposures for standard and compressed schedules were quite analogous. Although not shown in Fig. 2B, under these dosing schedules and using the base variable set in Table 2, normal brain and CSF concentrations were similar to those in brain tumors with the AUC_{bt}/AUC_{nb} of 1.0 and AUC_{bt}/AUC_{csf} of 1.2. An inference could be made that due to the close agreement in CSF and brain tumor temozolomide concentrations, monitoring of temozolomide CSF concentrations in patients could be used as a surrogate for brain tumor measurements due to its access and provide a rational basis to adjust doses. However, as supported by our simulations, individual patients may have different tumor characteristics, in this case due to either BBB permeability or tumor blood volume, which could alter the brain tumor distribution of temozolomide (Fig. 3). These changes in the brain tumor accumulation of temozolomide are not reflected in CSF and would argue against the use of CSF measurements as a brain tumor surrogate.

Temozolomide is an important drug for the treatment of brain tumors (2) and is a component in ongoing experimental

chemotherapeutic investigations to improve patient response and lower toxicity. The derived physiologically based pharmacokinetic model of temozolomide could be a component in future clinical studies by predicting temozolomide brain concentrations under different conditions, either due to new dosing schedules or due to a patient's physiologic state. Beyond the potential attributes of the human temozolomide pharmacokinetic model in brain, the strategy of developing a comprehensive rodent pharmacokinetic model able to be scaled to man offers a viable means to focus on target tissue drug concentrations, which may better reflect pharmacodynamic behavior.

References

1. Newlands ES, Blackledge GR, Slack JA, et al. Phase I trial of temozolomide (CCRG 81045: M&B 39831: NSC 362856). Br J Cancer 1992;65:287–91.
2. Mutter N, Stupp R. Temozolomide: a milestone in neuro-oncology and beyond? Expert Rev Anticancer Ther 2006;6:1187–204.
3. Jen JF, Cutler DL, Pai SM, et al. Population pharmacokinetics of temozolomide in cancer patients. Pharm Res 2000;17:1284–9.
4. Baker SD, Wirth M, Statkevich P, et al. Absorption, metabolism, and excretion of ^{14}C-temozolomide following oral administration to patients with advanced cancer. Clin Cancer Res 1999;5:309–17.
5. Ma J, Fei ZL, Klein-Szanto A, Gallo JM. Modulation of angiogenesis by human glioma xenograft models that differentially express vascular endothelial growth factor. Clin Exp Metastasis 1998;16:559–68.
6. Ma J, Pulfer S, Li S, Chu J, Reed K, Gallo JM. Pharmacodynamic-mediated reduction of temozolomide tumor concentrations by the angiogenesis inhibitor TNP-470. Cancer Res 2001;61:5491–8.
7. Paxinos G, Watson C. The rat brain in stereotaxic coordinates 3rd ed. Amsterdam: Elsevier Academic Press; 1997.
8. Freireich EJ, Gehan EA, Rall DP, Schmidt LH, Skipper HE. Quantitative comparison of toxicity of anticancer agents in mouse, rat, hamster, dog, monkey, and man. Cancer Chemother Rep 1966;50:219–44.
9. Zhou Q, Gallo JM. *In vivo* microdialysis for PK and PD studies of anticancer drugs. AAPS J 2005;7:E659–67.
10. Zhou Q, Guo P, Wang X, Nuthalapati S, Gallo JM. Preclinical pharmacokinetic and pharmacodynamic evaluation of metronomic and conventional temozolomide dosing regimens. J Pharmacol Exp Ther 2007;321:265–75.
11. Barrett PH, Bell BM, Cobelli C, et al. SAAM II: simulation, analysis, and modeling software for tracer and pharmacokinetic studies. Metabolism 1998;47:484–92.
12. SAAM II and PopKinetics, version 1.0b. Seattle (WA): University of Washington; 1999-2001.
13. Ostermann S, Csajka C, Buclin T, et al. Plasma and cerebrospinal fluid population pharmacokinetics of temozolomide in malignant glioma patients. Clin Cancer Res 2004;10:3728–36.
14. Kawakami J, Yamamoto K, Sawada Y, Iga T. Prediction of brain delivery of ofloxacin, a new quinolone, in the human from animal data. J Pharmacokinet Biopharm 1994;22:207–27.
15. Davies B, Morris T. Physiological parameters in laboratory animals and humans Physiological parameters in laboratory animals and humans. Pharm Res 1993;10:1093–5.
16. Warmuth C, Gunther M, Zimmer C. Quantification of blood flow in brain tumors: comparison of arterial spin labeling and dynamic susceptibility-weighted contrast-enhanced MR imaging. Radiology 2003;228:523–32.
17. Law M, Yang S, Babb JS, et al. Comparison of cerebral blood volume and vascular permeability from dynamic susceptibility contrast-enhanced perfusion MR imaging with glioma grade. AJNR Am J Neuroradiol 2004;25:746–55.
18. Collins JM, Dedrick RL. Distributed model for drug delivery to CSF and brain tissue. Am J Physiol 1983;245:R303–10.
19. Denny BJ, Wheelhouse RT, Stevens MF, Tsang LL, Slack JA. NMR and molecular modeling investigation of the mechanism of activation of the antitumor drug temozolomide and its interaction with DNA. Biochemistry 1994;33:9045–51.
20. Fross RD, Warnke PC, Groothuis DR. Blood flow and blood-to-tissue transport in 9L gliosarcomas: the role of the brain tumor model in drug delivery research. J Neurooncol 1991;11:185–97.
21. Uematsu H, Maeda M. Double-echo perfusion-weighted MR imaging: basic concepts and application in brain tumors for the assessment of tumor blood volume and vascular permeability. Eur Radiol 2006;16:180–6.
22. Schlageter KE, Molnar P, Lapin GD, Groothuis DR. Microvessel organization and structure in experimental brain tumors: microvessel populations with distinctive structural and functional properties. Microvasc Res 1999;58:312–28.
23. Gallo JM, Vicini P, Orlansky A, et al. Pharmacokinetic model-predicted anticancer drug concentrations in human tumors. Clin Cancer Res 2004;10:8048–58.
24. Gallo JM, Li S, Guo P, Reed K, Ma J. The effect of P-glycoprotein on paclitaxel brain and brain tumor distribution in mice. Cancer Res 2003;63:5114–7.
25. Lin JH, Lu AY. Role of pharmacokinetics and metabolism in drug discovery and development. Pharmacol Rev 1997;49:403–49.
26. Pardridge WM. Drug delivery to the brain. J Cereb Blood Flow Metab 1997;17:713–31.
27. Keep RF, Jones HC. A morphometric study on the development of the lateral ventricle choroid plexus, choroid plexus capillaries, and ventricular ependyma in the rat. Brain Res Dev Brain Res 1990;56:47–53.
28. Speake T, Brown PD. Ion channels in epithelial cells of the choroid plexus isolated from the lateral ventricle of rat brain. Brain Res 2004;1005:60–6.
29. Cao Y, Sundgren PC, Tsien CI, Chenevert TT, Junck L. Physiologic and metabolic magnetic resonance imaging in gliomas. J Clin Oncol 2006;24:1228–35.
30. Boxenbaum H, Ronfeld R. Interspecies pharmacokinetic scaling and the Dedrick plots. Am J Physiol 1983;245:R768–75.
31. Holleran JL, Parise RA, Joseph E, et al. Plasma pharmacokinetics, oral bioavailability, and interspecies scaling of the DNA methyltransferase inhibitor, zebularine. Clin Cancer Res 2005;11:3862–8.
32. Charnick SB, Kawai R, Nedelman JR, Lemaire M, Niederberger W, Sato H. Perspectives in pharmacokinetics. Physiologically based pharmacokinetic modeling as a tool for drug development. J Pharmacokinet Biopharm 1995;23:217–29.
33. Mordenti J. Man versus beast: pharmacokinetic scaling in mammals. J Pharm Sci 1986;75:1028–40.
34. Ward KW, Smith BR. A comprehensive quantitative and qualitative evaluation of extrapolation of intravenous pharmacokinetic parameters from rat, dog, and monkey to humans. I. Clearance. Drug Metab Dispos 2004;32:603–11.

Clinical Cancer Research

Predicting Human Tumor Drug Concentrations from a Preclinical Pharmacokinetic Model of Temozolomide Brain Disposition

Qingyu Zhou, Ping Guo, Gary D. Kruh, et al.

Clin Cancer Res 2007;13:4271-4279.